

# Efficient Electrochemical Water Oxidation by a Trinuclear Ru(bda) Macrocycle Immobilized on Multi-Walled Carbon Nanotube Electrodes

Dorothee Schindler, Marcos Gil-Sepulcre, Joachim O. Lindner, Vladimir Stepanenko, Dooshaye Moonshiram, Antoni Llobet,\* and Frank Würthner\*

Catalytic water splitting is a viable process for the generation of renewable fuels. Here it is reported for the first time that a trinuclear supramolecular Ru(bda) (bda: 2,2'-bipyridine-6,6'-dicarboxylate) catalyst, anchored on multi-walled carbon nanotubes and subsequently immobilized on glassy carbon electrodes, shows outstanding performance in heterogeneous water oxidation. Activation of the catalyst on anodes by repetitive cyclic voltammetry (CV) scans results in a catalytic current density of 186 mA cm<sup>-2</sup> at a potential of 1.45 V versus NHE. The activated catalyst performs water oxidation at an onset overpotential of 330 mV. The remarkably high stability of the hybrid anode is demonstrated by X-ray absorption spectroscopy and electrochemically, revealing the absence of any degradation after 1.8 million turnovers. Foot of the wave analysis of CV data of activated electrodes with different concentrations of catalyst indicates a monomolecular water nucleophilic attack mechanism with an apparent rate constant of TOF<sub>max</sub> (turnover frequency) of 3200 s<sup>-1</sup>.

Natural photosynthesis has inspired in the last decades many novel approaches for the generation of renewable fuels.<sup>[1]</sup> In this regard, catalytic water splitting into molecular oxygen and hydrogen is a highly promising process.<sup>[2]</sup> Toward this goal, however, efficient water oxidation catalysts (WOCs) are required to overcome the high energy barriers of the demanding anodic half reaction of water oxidation into molecular oxygen.<sup>[3]</sup> Indeed, considerable progress has been made over the last decades in the development of molecular WOCs and valuable mechanistic understanding of catalytic water oxidation has been acquired.<sup>[3c,4]</sup> In particular, the class of molecular Ru(bda) catalysts (bda: [2,2'-bipyridine]-6,6'-dicarboxylate) has shown high catalytic efficiencies comparable to nature's oxygen evolving complex.<sup>[4b,5]</sup> However, for the

implementation of such WOCs in water splitting devices their immobilization on proper surfaces is required.<sup>[6]</sup>

For the immobilization of homogeneous WOCs onto electrodes, mainly two strategies have been employed. One of them is based on covalent attachment of molecular catalysts to electrode surfaces by silane-, carboxylate-, or phosphonate-functionalized ligands.<sup>[7]</sup> Another approach is a supramolecular one, comprising introduction of aromatic groups to the WOCs to facilitate non-covalent  $\pi$ - $\pi$  interactions between the catalyst and a supporting material like carbon nanotubes (CNTs).<sup>[8]</sup> Due to their large surface area as well as high conductivity and stability,<sup>[9]</sup> CNTs are properly suited for immobilization of catalysts on electrodes. Cao and co-workers compared different linking strategies of Co corroles on CNTs and reported improved activities and the importance of fast electron transfer for high efficiencies.<sup>[10]</sup> Indeed, Sun and co-workers have shown that a derivative of Ru(bda)(pic)<sub>2</sub> WOC, containing axial pyridyl ligands that are functionalized with pyrene groups through amide linkers, can be immobilized on multi-walled carbon nanotubes (MWCNTs).<sup>[8a]</sup> Recently, some of us have also successfully anchored a Ru(tda) (tda: [2,2':6',2"-terpyridine]-6,6'-dicarboxylate) catalyst bearing pyrene-functionalized axial ligands on MWCNTs by  $\pi$ - $\pi$  interactions and demonstrated heterogeneous water oxidation for this hybrid material.<sup>[8b]</sup> It has been reported in the literature that immobilization of molecular Ru(bda) catalysts, which operate by I2M (interaction of two M-O units) mechanism<sup>[11]</sup> in homogeneous phase


D. Schindler, Dr. V. Stepanenko, Prof. F. Würthner  
Institut für Organische Chemie  
Universität Würzburg  
Am Hubland, Würzburg 97074, Germany  
E-mail: wuerthner@uni-wuerzburg.de

Dr. M. Gil-Sepulcre, Prof. A. Llobet  
Institut Català d'Investigació Química (ICIQ)  
Barcelona Institute of Science and Technology (BIST)  
Avinguda Països Catalans 16, Tarragona 43007, Spain  
E-mail: allobet@iciq.cat

Dr. J. O. Lindner, Dr. V. Stepanenko, Prof. F. Würthner  
Center for Nanosystems Chemistry  
Theodor-Boveri-Weg, Würzburg 97074, Germany

Dr. D. Moonshiram  
Instituto Madrileño de Estudios Avanzados en Nanociencia  
(IMDEA Nanociencia)  
Calle Faraday, 9, Madrid 28049, Spain

Prof. A. Llobet  
Departament de Química  
Universitat Autònoma de Barcelona  
Cerdanyola del Vallès, Barcelona 08193, Spain

 The ORCID identification number(s) for the author(s) of this article can be found under <https://doi.org/10.1002/aenm.202002329>.

© 2020 The Authors. Published by Wiley-VCH GmbH. This is an open access article under the terms of the Creative Commons Attribution-NonCommercial-NoDerivs License, which permits use and distribution in any medium, provided the original work is properly cited, the use is non-commercial and no modifications or adaptations are made.

DOI: 10.1002/aenm.202002329

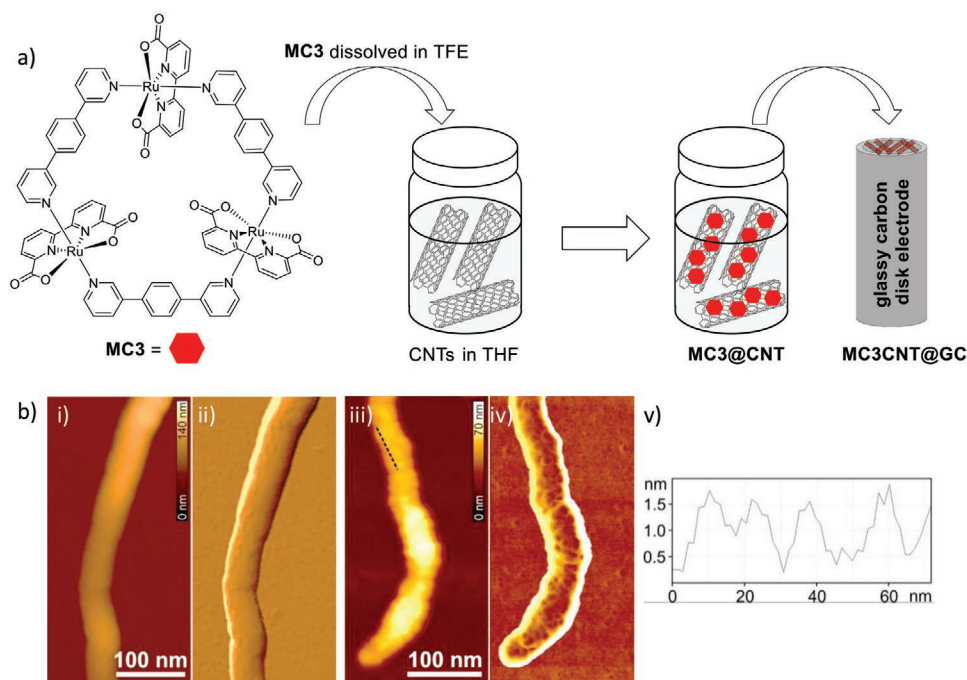


**Figure 1.** a) Structure of the Ru(bda) macrocycle MC3 and schematic illustration of its immobilization on CNTs and subsequent deposition onto a glassy carbon disk. b) AFM images obtained after spin coating a dispersion of MWCNTs and MC3@CNT (1 mg of CNT in 1 mL THF and with the addition of 0.2 mL of MC3 in TFE ( $c = 1 \text{ mg mL}^{-1}$ )) onto a silicon wafer: i) Height of bare CNT, Z scale is 115 nm, ii) phase image of bare CNT, iii) height of CNT decorated with MC3, Z scale is 70 nm, iv) phase image of CNT decorated with MC3, and v) cross-section profile of section marked with black dotted line in image (iii).

on electrodes, leads to adverse effects on their catalytic activity in heterogeneous catalysis<sup>[12]</sup> due to restricted mobility, associated with a switch to the water nucleophilic attack (WNA) mechanism.<sup>[11]</sup> This implies that Ru-based WOCs functioning through the latter mechanism are favorable for heterogeneous catalysis.<sup>[13]</sup>

Thus, we envisioned that macrocyclic WOCs bearing three Ru(bda) units such as MC3 (highly soluble in a  $\text{CH}_2\text{Cl}_2/\text{MeOH}$  [5:3] mixture but not in pure water, for structure see **Figure 1a**) should be a promising candidate for heterogeneous water oxidation as MC3 exhibits high catalytic efficiency in homogeneous water oxidation via a WNA mechanism<sup>[14]</sup> and benefits from the supramolecular arrangement.<sup>[15]</sup> As this metallomacrocycle comprises three linear aromatic linker ligands in addition to the three bda units, we assumed that it should be possible to anchor this catalyst on CNTs by non-covalent  $\pi$ - $\pi$  and  $\text{CH}-\pi$  interactions toward the graphene-like surface without further functionalization for heterogeneous catalytic water oxidation.<sup>[16]</sup> Here we report that MC3 indeed adheres to CNTs as confirmed by electrochemical techniques and atomic force microscopy (AFM). More importantly, CNT-anchored MC3 immobilized on glassy carbon electrodes performed outstanding catalytic activity in electrochemically driven water oxidation underlining its potential for device application.

To anchor trinuclear Ru(bda) catalyst MC3 on MWCNT surface, 0.1 mL of a solution of MC3 in trifluoroethanol (TFE) was added to a freshly prepared dispersion of MWCNTs in THF (**Figure 1a**). Immediate decolorization of the mixture indicated the binding of the catalyst onto the surface of the CNTs. To

confirm that catalyst MC3 is indeed attached to the CNTs, AFM measurements were performed by spin coating a dispersion of MC3@CNT onto a silicon wafer (**Figure 1b**). In comparison to a bare CNT (**Figure 1b-i,ii**), magnification and height profile of one single CNT decorated with MC3 (**Figure 1b-iii-v**) clearly shows the distribution of the anchored MC3 molecules on the nanotube surface. Thus, for the first time we could prove by a microscopic method direct anchoring of an unfunctionalized Ru(bda) complex to CNTs through non-covalent interactions. Further characterization by scanning electron microscopy and energy-dispersive X-ray spectroscopy experiments (**Figures S1-S3**, Supporting Information) was performed to characterize MC3@CNTs. Investigations of the coverage on a well-defined glassy carbon disk demonstrate that 93% of the surface are covered, indicating the formation of a monolayer distribution on the carbon material (**Figure S4**, Supporting Information).

For electrochemical studies, working electrodes (WE) were prepared by drop-casting a suspension of MC3@CNT onto glassy carbon disk electrodes ( $S = 0.07 \text{ cm}^2$ , denoted as MC3@CNT@GC). Cyclic voltammetry (CV) experiments were then performed with these electrodes in a 1 M phosphate buffer solution (pH 7) using a three electrode cell. A platinum mesh and Hg/HgSO<sub>4</sub> electrode were used as counter (CE) and reference electrodes (RE), respectively. All potentials reported hereinafter are converted and referenced to NHE. The catalytic process was initiated at an onset potential of 1.05 V (**Figure S5**, Supporting Information) and current densities of about  $50 \text{ mA cm}^{-2}$  at  $E = 1.45 \text{ V}$  were observed in the first cycle (**Figure 2c**, black line). Repetitive CV cycles up to a

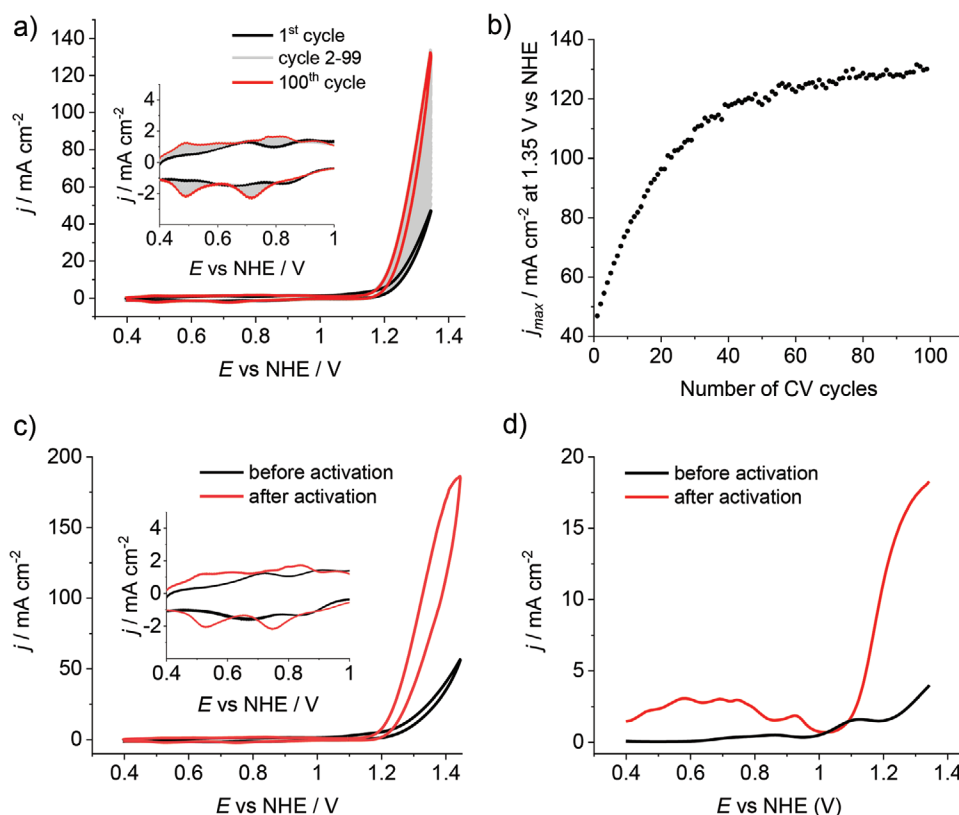


**Figure 2.** Electrochemical experiments with MC3@CNT@GC in 1 M phosphate buffer (pH 7). a) 100 repetitive CV scans (scan rate: 100 mV s<sup>-1</sup>). Inset: Enlarged area of the non-catalytic waves. Initial scan in the first cycle is shown in black, 100th cycle is shown in red. Scans 2–99 are depicted in grey. b) Development of the maximal current densities at  $E = 1.35$  V versus NHE with the increasing number of CV scans. c) Comparison of the cyclic voltammograms (scan rate: 100 mV s<sup>-1</sup>) of the initial (black line) and the final species (red line) after 100 CV cycles. d) Comparison of the differential pulse voltammograms of the initial species (black line) and the final species after 100 CV cycles (red line).

potential of 1.35 V revealed a steady rise of the catalytic current (Figure 2a,b), along with changes in the non-catalytically active redox waves (Figure 2a, inset). As the number of CV cycles increases, higher catalytic current densities are observed until a plateau is reached after around 100 cycles (Figure 2b).

Control CV experiments confirmed that CNT decorated electrode without the catalyst (CNT@GC, Figure S6a, Supporting Information, blank) does not produce any significant current under identical experimental conditions. Notably, MC3 as a homogeneous catalyst in a phosphate buffer/TFE 1:1 mixture (pH 7) does not show any comparable catalytic activity in water oxidation (Figure S6b, Supporting Information). Investigations of the redox properties of homogeneous MC3 by differential pulse voltammetry (DPV) showed three reversible oxidation processes that are assignable to the transitions from the Ru<sup>II</sup> to Ru<sup>V</sup> oxidation states.<sup>[14a]</sup> DPV analysis of MC3@CNT@GC electrode revealed that the first and the second oxidation waves of immobilized MC3 correspond to the Ru<sup>III/II</sup> and Ru<sup>IV/III</sup> redox couples at  $E = 0.68$  and 0.85 V, respectively, and are not influenced by the immobilization of the catalyst. The Ru<sup>V/IV</sup> oxidation is shifted to higher potentials from 1.02 to 1.11 V in the case of MC3@CNT@GC compared to the non-immobilized catalyst (Figure S6c,d, Supporting Information).

By DPV analysis, the appearance of additional redox waves of MC3@CNT@GC and a rise in the catalytic current can be

observed after the final state is reached upon 100 CV cycles (Figure 2d). This indicates the formation of a new and even more active species on the electrode. Five redox processes can be seen before the onset of the WOC, which is now shifted to higher potentials and appears at  $E_{\text{onset}} = 1.15$  V, giving an overpotential of 330 mV for water oxidation. The Ru<sup>V/IV</sup> oxidation of the initial species is covered by the catalytic slope of the newly formed species and, therefore, not observable any more. The first redox process of the newly formed species arises at 0.50 V, which presumably corresponds to the Ru<sup>III/II</sup> redox process and is also shifted to lower potentials than in the initial species. Similar electrochemical activation processes have already been described for other Ru catalysts like Ru(tda)(py)<sub>2</sub> (tda = [2,2':6',2''-terpyridine]-6,6''-dicarboxylate) or Ru(pdc)(bpy)<sub>2</sub> (pdc: pyridyl-2,6-dicarboxylate),<sup>[4c,17]</sup> where the formation of a Ru aqua species as active catalyst was supposed after repetitive CV cycles. However, such activated species have not been reported for Ru(bda) catalysts. X-ray absorption (XAS) spectroscopy provides further evidence of the molecularity of the water oxidation active catalyst since no RuO<sub>2</sub> can be detected at the surface of the electrode after catalysis (Figure S7, Tables S1–S3, Supporting Information).

After removing all oxygen bubbles from the surface of the activated electrodes (act-MC3@CNT@GC), a cyclic voltammogram was recorded and compared to one of the unactivated

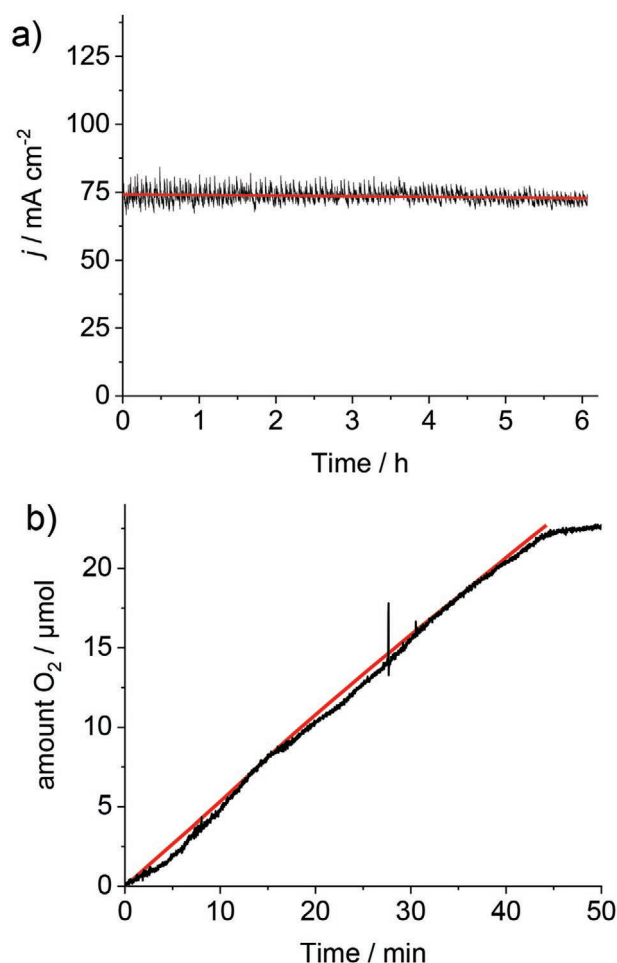


**Figure 3.** a) Controlled potential electrolysis (CPE) experiment of activated electrode act-MC3@CNT@GC in a 1 M phosphate buffer (pH 7) at 1.6 V versus NHE for 6 h. b) Determination of the Faraday efficiency. The red line shows the theoretical amount of produced oxygen calculated from the passed charge in a CPE experiment assuming a Faraday efficiency of 100%. The black line corresponds to the head-space analysis of the amount of oxygen detected by a Clark electrode.

electrode (MC3@CNT@GC, Figure 2c). An exceptionally high current density ( $j$ ) of  $186 \text{ mA cm}^{-2}$  was reached at  $E = 1.45 \text{ V}$  after the activation process, which is about four times higher than the value observed before activation (Figure 2c, average in three independent experiments:  $176 \text{ mA cm}^{-2}$ , Figure S8, Supporting Information). Earlier approaches by Sun and co-workers on an ITO surface using CNTs as support resulted in current densities of only  $720 \mu\text{A cm}^{-2}$ .<sup>[8a]</sup> Thus, the observed  $j_{\text{max}}$  value for anchored and activated MC3 is the highest one reported so far for Ru(bda) catalysts with confirmed molecular active species and comparable with the very recently observed maximum current density of  $240 \text{ mA cm}^{-2}$  for an immobilized Ru(tda) polymer.<sup>[6]</sup>

Proven to be highly efficient, the stability and efficiency of the act-MC3@CNT@GC electrodes was then investigated by controlled potential electrolysis (CPE) experiments (Figure 3). A two-compartment setup was used, where the working and

the reference electrodes were placed in one chamber and the counter electrode in the other one. A constant potential of 1.6 V was applied. No decrease in the catalytic current during 6 h confirms that the immobilized catalyst does not undergo any considerable degradation or detachment from the electrode during continuous catalytic water oxidation process (Figure 3a). With only a negligible loss, 97% of the initial current density still remains after 6 h. No significant changes in the CV were observed before and after this experiment, confirming the high stability of the activated species (Figure S9a, Supporting Information).

Assuming that all electrons passing through the system are involved in the catalytic reaction, the amount of generated oxygen can be calculated from the charge after 6 h (Figure S9b, Supporting Information). According to the water oxidation reaction and assuming 100% Faraday efficiency (which will be confirmed below), four electrons are used to generate one molecule of oxygen. Therefore, the amount of generated oxygen was calculated from the passed charge by employing Faraday law to be  $2.6 \times 10^{-4} \text{ mol}$  and divided by the total amount of Ru centers after activation ( $1.44 \times 10^{-10} \text{ mol}$ ) on the electrode. The details for this determination are given in Figures S9 and S10, Supporting Information and description given under Figure S10, Supporting Information. These values lead to a remarkably high turnover number (TON) of 1.8 million referred to activated Ru on the electrode (0.5 million with respect to the total amount of Ru on the electrode before activation (Figure S10d, Supporting Information)). Assigning the first oxidation process in the CV after activation to the one-electron transfer process of the Ru<sup>III/II</sup> oxidation in every Ru(bda) center of the trinuclear Ru(bda) complex MC3, the amount of Ru on the surface of the act-MC3@CNT@GC electrode can be determined by integrating the area under the respective waves in the cathodic and anodic scan (Figure S10a–c, Supporting Information).

To verify that no side processes other than water oxidation take place during this electrochemical reaction and all electrons are involved in the water oxidation, the Faraday efficiency of act-MC3@CNT@GC was determined. The amount of charge passing through the system was recorded by the potentiostat and the actual amount of oxygen produced during one CPE experiment was measured by a gas phase Clark electrode in the head space of the chamber containing the working electrode. For this purpose, a glassy carbon plate was used as a working electrode due to its increased surface area. A constant potential of 1.3 V was applied, and after few seconds bubbles of oxygen could be seen by the naked eye on the working electrode. The CPE experiment was stopped after 45 min. The quantity of detected oxygen was compared to the theoretical maximum calculated one, assuming a Faraday efficiency of 100% (for details see Methods in Supporting Information). Almost no deviations between these values (Figure 3b) imply a Faraday efficiency of 99%.

The foot of the wave analysis (FOWA), first developed by Savéant and co-workers<sup>[18]</sup> and applied for electrocatalytic reduction processes<sup>[19]</sup> and later adapted to the electrochemical water oxidation,<sup>[13a]</sup> was performed to gain more insights into the kinetics of the electrocatalytic water oxidation reaction performed by act-MC3@CNT@GC (Figure 4). Electrodes with different loadings of the catalyst were prepared, activated, and

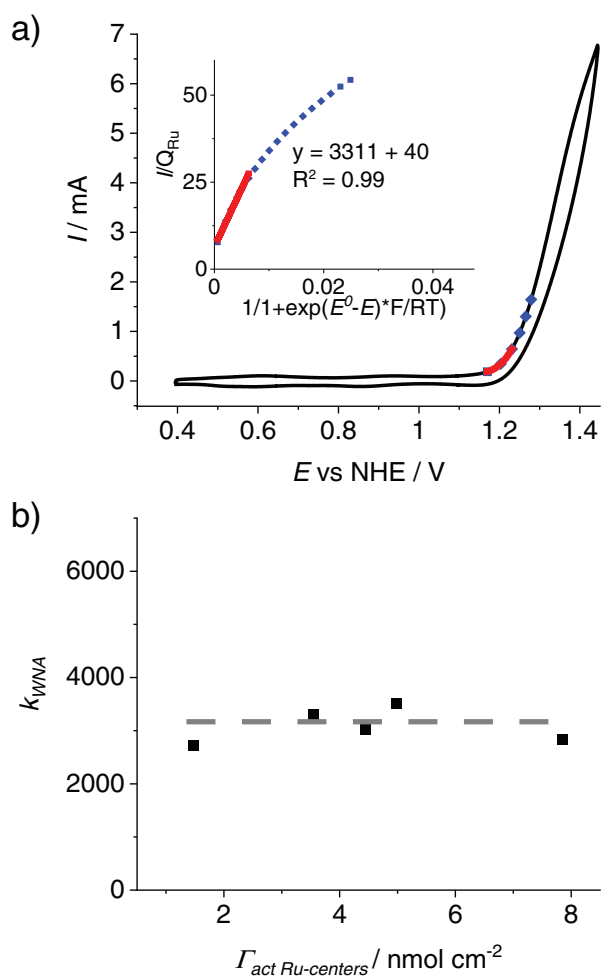


**Figure 4.** a) The solid black line shows the second cycle of the CV of act-MC3@CNT@GC in a 1 M phosphate buffer (pH 7) for a surface concentration of the active species of  $\Gamma_{\text{act cat}} = 2.4 \text{ nmol cm}^{-2}$ . The region used for the FOWA is indicated by the blue dotted line. The red solid line at the foot of the wave (1.17–1.23 V) shows the area which is used for the determination of the apparent rate constant. Inset:  $i/Q_{\text{Ru}}$  versus  $1/(1 + \exp(E^0 - E) * F/RT)$  plot assuming a WNA mechanism for the immobilized macrocyclic catalyst. The apparent rate constant  $k_{\text{WNA}}$  at the foot of the wave was obtained by fitting the points represented by the solid red line. b) The  $k_{\text{WNA}}$  values obtained from  $i/Q_{\text{Ru}}$  versus  $1/(1 + \exp(E^0 - E) * F/RT)$  plot (a, inset) at the corresponding surface concentrations of the active species are shown as black data points. Independence of the  $k_{\text{WNA}}$  values of the surface concentration indicated by the grey dashed line is in agreement with the assumption of a WNA mechanism on the surface.

subsequently CV experiments were performed at operating potentials of 0.4–1.45 V (Figure 4a; Figure S11, Supporting Information) in order to apply the FOWA methodology.

For the extraction of the kinetic data, the first data points of the catalytic slope of one CV cycle (Figure 4a, blue dots) were used. The charge corresponding to one Ru oxidation event ( $Q_{\text{Ru}}$ ) was determined by integration of the area under the wave corresponding to the  $\text{Ru}^{\text{III/II}}$  oxidation process of the active species (Figure S10, Supporting Information). By assuming a hetero-WNA mechanism taking place on the electrode surface, these data points were plotted according to

$i/Q_{\text{Ru}}$  versus  $1/(1 + \exp(E^0 - E) * F/RT)$  (Figure 4a, inset; for details see Methods in Supporting Information and Equation (S1)). The gradient of the received curve was fitted by linear regression (Figure 4a, inset; red line). Its slope represents the apparent pseudo-rate constant ( $k_{\text{WNA}}$  value) at the foot of the catalytic wave for each electrode with different catalyst loadings, which equals the  $\text{TOF}_{\text{max}}$  value (see Methods in Supporting Information and Equation (S2)). The independence of  $k_{\text{WNA}}$  values versus surface concentration of the activated Ru centers (Figure 4b) is a clear indication of a single mechanism operating in this system. Further, the first-order kinetics with regards to the catalyst's concentration agrees with a WNA mechanism taking place for act-MC3@CNT@GC. An average apparent rate constant of  $k_{\text{WNA}} = \text{TOF}_{\text{max}} = (3197 \pm 395) \text{ s}^{-1}$  was obtained (Figure 4b), which is among the highest values reported so far for Ru-based WOCs (Table S4, Supporting Information). It has been reported in the literature that a  $\text{Ru}(\text{bda})(\text{L})_2$  catalyst (L = functionalized pyridine ligand), which oxidizes water via a bimolecular I2M O–O bond formation step in homogeneous catalysis, not only drops in activity, when immobilized on an electrode surface changing to a WNA mechanism (FOWA:  $\text{TOF}_{\text{max}} = 53 \text{ s}^{-1}$  homogeneous;  $\text{TOF}_{\text{max}} = 1.9 \text{ s}^{-1}$  heterogeneous), but also ends up decomposing to  $\text{RuO}_2$ .<sup>[12,13]</sup> In contrast, a  $\text{Ru}(\text{tda})(\text{L})_2$  catalyst which functions through a WNA mechanism in homogeneous catalysis does not undergo any significant change upon immobilization (FOWA:  $\text{TOF}_{\text{max}} = 8000 \text{ s}^{-1}$  homogeneous;  $\text{TOF}_{\text{max}} = 9000 \text{ s}^{-1}$  heterogeneous).<sup>[8b,12a]</sup> The latter is also the case for our trinuclear  $\text{Ru}(\text{bda})$  macrocycle MC3, which was previously reported to function through a WNA mechanism.<sup>[14a]</sup> Since activation of MC3 is only observed upon its adsorption on MWCNTs, the strength of non-covalent interactions with the CNT surface is assumed to play a crucial role during this process. Indeed, our semiempirical calculations using graphene-like surface as a model indicated that a structure with partial decoordination of bda ligands, allowing for the coordination of additional water molecules to Ru (Figure 5; Figure S12, Supporting Information), introduces additional stabilizing  $\pi$ – $\pi$  interactions compared to different possible conformations of MC3 (Figure S13, Supporting Information). Owing to the presence of multiple acidic protons in the environment of aqua-coordinated Ru, oxidation of this species up to  $\text{Ru}^{\text{V}}$  is possible without total charge buildup (Figure S14, Supporting Information). Such diaqua species would explain the

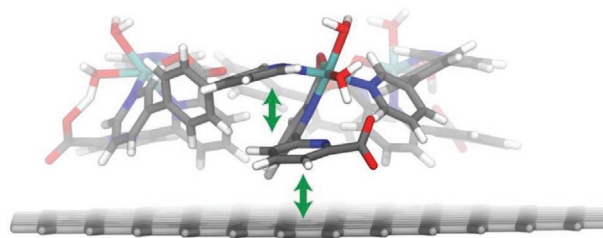


**Figure 5.** Optimized structure based on semiempirical calculations of the proposed activated species act-MC3@CNT@GC (grey: carbon, white: hydrogen, blue: nitrogen, red: oxygen, turquoise: ruthenium). A hexagonal graphene sheet has been used as a model for the graphitic surface of MWCNTs. Cartesian coordinates are provided in Table S5, Supporting Information. For computational details, see Methods in Supporting Information. Green double-headed arrows indicate attractive  $\pi$ – $\pi$  interactions.

observed, notably changed redox behavior of act-MC3@CNT@GC compared to the non-activated MC3@CNT@GC and may play a role in electrochemical heterogeneous water oxidation by Ru(bda) macrocycle.

In conclusion, we have successfully immobilized our macrocyclic MC3 catalyst onto CNTs as confirmed by electrochemical techniques and AFM images. Taking advantage of the intrinsic properties of CNTs, glassy carbon electrodes with anchored MC3 catalyst were prepared. To the best of our knowledge, this is the first report of an electrochemical activation of a Ru(bda) complex that has been transformed into a more active species by repetitive CV cycles. A current density as high as 186 mA cm<sup>-2</sup> was observed, which is among the highest values reported so far for molecular Ru catalysts anchored on solid state anodes. A Faraday efficiency of 99% together with XAS spectroscopy demonstrates that the activated species does not undergo any unproductive side reactions during the catalytic process and neither leads to the formation of RuO<sub>2</sub>. With a remarkably high TON value of 1.8 million and a TOF<sub>max</sub> of 3200 s<sup>-1</sup> the act-MC3@CNT@GC electrodes are efficient devices for electrochemically driven heterogeneous water oxidation.

## Supporting Information

Supporting Information is available from the Wiley Online Library or from the author.

## Acknowledgements

This project has received funding from the European Research Council (ERC) under the European Union's Horizon 2020 research and innovation programme (grant agreement no. 787937; recipient F.W.). The authors thank the Alexander von Humboldt foundation for supporting this collaborative research with a Humboldt research award for A.L. A.L. also acknowledges support from Ministerio de Ciencia e Innovación, FEDER, and AGAUR through grants: PID2019-111617RB-I00 and 2017-SGR-163. D.M. acknowledges funding from the Severo Ochoa Excellence program (SE2016-06860686), from the Instituto IMDEA Nanociencia, the Acciones de Dinamización "Europa Investigación" grant (EIN2019-103399), and the Spanish Ministerio de Ciencia, Innovación y Universidades grant (PID2019-111086RA-I00). This research used resources of the Advanced Photon Source (Beamline 9 BM-B), an Office of Science User Facility operated for the US Department of Energy (DOE) Office of Science by Argonne National Laboratory, and was supported by the US DOE under Contract No. DE-AC02-06CH11357.

Open access funding enabled and organized by Projekt DEAL.

## Conflict of Interest

The authors declare no conflict of interest.

## Keywords

electrocatalysis, heterogeneous catalysis, renewable fuels, ruthenium bda complexes, water splitting

Received: July 17, 2020

Revised: September 4, 2020

Published online: October 4, 2020

- [1] a) P. D. Frischmann, K. Mahata, F. Würthner, *Chem. Soc. Rev.* **2013**, *42*, 1847; b) S. Berardi, S. Drouet, L. Francas, C. Gimbert-Suriñach, M. Guttentag, C. Richmond, T. Stoll, A. Llobet, *Chem. Soc. Rev.* **2014**, *43*, 7501; c) B. Zhang, L. Sun, *Chem. Soc. Rev.* **2019**, *48*, 2216; d) M. G. Walter, E. L. Warren, J. R. McKone, S. W. Boettcher, Q. Mi, E. A. Santori, N. S. Lewis, *Chem. Rev.* **2010**, *110*, 6446; e) R. J. Detz, K. Sakai, L. Spiccia, G. W. Brudvig, L. Sun, J. N. H. Reek, *ChemPlusChem* **2016**, *81*, 1024; f) T. Sharifi, C. Larsen, J. Wang, W. L. Kwong, E. Gracia-Espino, G. Mercier, J. Messinger, T. Wågberg, L. Edman, *Adv. Energy Mater.* **2016**, *6*, 1600738.
- [2] a) M. Beller, G. Centi, L. Sun, *ChemSusChem* **2017**, *10*, 6; b) A. Llobet, *Molecular Water Oxidation Catalysis: A Key Topic for New Sustainable Energy Conversion Schemes*, John Wiley and Sons Ltd., New York **2014**; c) J. O. M. Bockris, *Materials* **2011**, *4*, 2073; d) J. Qi, W. Zhang, R. Cao, *Adv. Energy Mater.* **2018**, *8*, 1701620; e) J. R. McKone, N. S. Lewis, H. B. Gray, *Chem. Mater.* **2014**, *26*, 407.
- [3] a) J. Hessels, R. J. Detz, M. T. M. Koper, J. N. H. Reek, *Chem. - Eur. J.* **2017**, *23*, 16413; b) A. Kudo, Y. Miseki, *Chem. Soc. Rev.* **2009**, *38*, 253; c) S. Ye, C. Ding, M. Liu, A. Wang, Q. Huang, C. Li, *Adv. Mater.* **2019**, *31*, 1902069.
- [4] a) D. Moonshiram, V. Purohit, J. J. Concepcion, T. J. Meyer, Y. Pushkar, *Materials* **2013**, *6*, 392; b) B. Zhang, L. Sun, *J. Am. Chem. Soc.* **2019**, *141*, 5565; c) M. A. Hoque, J. Benet-Buchholz, A. Llobet, C. Gimbert-Suriñach, *ChemSusChem* **2019**, *12*, 1949; d) J. Shi, Y.-H. Guo, F. Xie, Q.-F. Chen, M.-T. Zhang, *Angew. Chem., Int. Ed.* **2020**, *59*, 4000.
- [5] L. Duan, F. Bozoglian, S. Mandal, B. Stewart, T. Privalov, A. Llobet, L. Sun, *Nat. Chem.* **2012**, *4*, 418.
- [6] a) R. Brimblecombe, G. C. Dismukes, G. F. Swiegers, L. Spiccia, *Dalton Trans.* **2009**, *43*, 9374; b) Z. Chen, J. J. Concepcion, J. W. Jurss, T. J. Meyer, *J. Am. Chem. Soc.* **2009**, *131*, 15580; c) L. Xie, X. Li, B. Wang, J. Meng, H. Lei, W. Zhang, R. Cao, *Angew. Chem., Int. Ed.* **2019**, *58*, 18883; d) F. Niu, D. Wang, F. Li, Y. Liu, S. Shen, T. J. Meyer, *Adv. Energy Mater.* **2020**, *10*, 1900399; e) J. Mola, E. Mas-Marza, X. Sala, I. Romero, M. Rodríguez, C. Viñas, T. Parella, A. Llobet, *Angew. Chem., Int. Ed.* **2008**, *47*, 5830.
- [7] a) Y. Gao, X. Ding, J. Liu, L. Wang, Z. Lu, L. Li, L. Sun, *J. Am. Chem. Soc.* **2013**, *135*, 4219; b) M. Yamamoto, Y. Nishizawa, P. Chabera, F. Li, T. Pascher, V. Sundstrom, L. Sun, H. Imahori, *Chem. Commun.* **2016**, *52*, 13702; c) L. Zhang, Y. Gao, X. Ding, Z. Yu, L. Sun, *ChemSusChem* **2014**, *7*, 2801; d) F. Li, K. Fan, L. Wang, Q. Daniel, L. Duan, L. Sun, *ACS Catal.* **2015**, *5*, 3786; e) F. L. Ke Fan, L. Wang, Q. Daniel, E. Gabrielsso, L. Sun, *Phys. Chem. Chem. Phys.* **2014**, *16*, 25234; f) J. Odobina, J. Scholz, M. Risch, S. Dechert, C. Jooss, F. Meyer, *ACS Catal.* **2017**, *7*, 6235.
- [8] a) F. Li, B. Zhang, X. Li, Y. Jiang, L. Chen, Y. Li, L. Sun, *Angew. Chem., Int. Ed.* **2011**, *50*, 12276; b) J. Creus, R. Matheu, I. Peñafiel, D. Moonshiram, P. Blondeau, J. Benet-Buchholz, J. García-Antón, X. Sala, C. Godard, A. Llobet, *Angew. Chem., Int. Ed.* **2016**, *55*, 15382.
- [9] a) N. Karousis, N. Tagmatarchis, D. Tasis, *Chem. Rev.* **2010**, *110*, 5366; b) V. Strauss, A. Roth, M. Sekita, D. M. Guldi, *Chem* **2016**, *1*, 531; c) V. Sgobba, D. M. Guldi, *Chem. Soc. Rev.* **2009**, *38*, 165; d) T. Umeyama, H. Imahori, *Energy Environ. Sci.* **2008**, *1*, 120.
- [10] a) X. Li, H. Lei, J. Liu, X. Zhao, S. Ding, Z. Zhang, X. Tao, W. Zhang, W. Wang, X. Zheng, R. Cao, *Angew. Chem., Int. Ed.* **2018**, *57*, 15070; b) J. Meng, H. Lei, X. Li, J. Qi, W. Zhang, R. Cao, *ACS Catal.* **2019**, *9*, 4551.
- [11] X. Sala, S. Maji, R. Bofill, J. García-Antón, L. Escriche, A. Llobet, *Acc. Chem. Res.* **2014**, *47*, 504.
- [12] a) P. Garrido-Barros, R. Matheu, C. Gimbert-Suriñach, A. Llobet, *Curr. Opin. Electrochem.* **2019**, *15*, 140; b) R. Matheu, L. Francàs, P. Chernev, M. Z. Ertem, V. Batista, M. Haumann, X. Sala, A. Llobet, *ACS Catal.* **2015**, *5*, 3422.
- [13] a) R. Matheu, S. Neudeck, F. Meyer, X. Sala, A. Llobet, *ChemSusChem* **2016**, *9*, 3361; b) D. W. Shaffer, Y. Xie, J. J. Concepcion, *Chem. Soc. Rev.* **2017**, *46*, 6170.

- [14] a) M. Schulze, V. Kunz, P. D. Frischmann, F. Würthner, *Nat. Chem.* **2016**, *8*, 576; b) V. Kunz, D. Schmidt, M. I. S. Röhr, R. Mitrić, F. Würthner, *Adv. Energy Mater.* **2017**, *7*, 1602939.
- [15] V. Kunz, J. O. Lindner, M. Schulze, M. I. S. Röhr, D. Schmidt, R. Mitrić, F. Würthner, *Energy Environ. Sci.* **2017**, *10*, 2137.
- [16] M. A. Hoque, M. Gil-Sepulcre, A. d. Aguirre, J. A. A. W. Elemans, D. Moonshiram, Y. S. R. Matheu, J. Benet-Buchholz, X. Sala, M. Malfois, E. Solano, J. Lim, A. Garzón-Manjón, C. Scheu, M. Lanza, F. Maseras, C. Gimbert-Suriñach, A. Llobet, *Nat. Chem.* **2020**, <https://doi.org/10.1038/s41557-020-0548-7>.
- [17] R. Matheu, M. Z. Ertem, J. Benet-Buchholz, E. Coronado, V. S. Batista, X. Sala, A. Llobet, *J. Am. Chem. Soc.* **2015**, *137*, 10786.
- [18] C. Costentin, S. Drouet, M. Robert, J.-M. Savéant, *J. Am. Chem. Soc.* **2012**, *134*, 11235.
- [19] a) C. Costentin, S. Drouet, M. Robert, J.-M. Savéant, *Science* **2012**, *338*, 90; b) V. Artero, J.-M. Savéant, *Energy Environ. Sci.* **2014**, *7*, 3808; c) C. Costentin, J.-M. Savéant, *ChemElectroChem* **2014**, *1*, 1226; d) C. Costentin, H. Dridi, J.-M. Savéant, *J. Am. Chem. Soc.* **2014**, *136*, 13727; e) C. Costentin, G. Passard, J.-M. Savéant, *J. Am. Chem. Soc.* **2015**, *137*, 5461.